Phase transitions in a system of hard Y-shaped particles on the triangular lattice

Dipanjan Mandal,[1,2,*] Trisha Nath,[3,†] and R. Rajesh[1,2,‡]

[1]*The Institute of Mathematical Sciences, C.I.T. Campus, Taramani, Chennai 600113, India*
[2]*Homi Bhabha National Institute, Training School Complex, Anushakti Nagar, Mumbai 400094, India*
[3]*Institut für Theoretische Physik, Georg-August-Universität Göttingen, 37077 Göttingen, Germany*

We study the different phases and the phase transitions in a system of Y-shaped particles, examples of which include immunoglobulin-G and trinaphthylene molecules, on a triangular lattice interacting exclusively through excluded volume interactions. Each particle consists of a central site and three of its six nearest neighbors chosen alternately, such that there are two types of particles which are mirror images of each other. We study the equilibrium properties of the system using grand canonical Monte Carlo simulations that implement an algorithm with cluster moves that is able to equilibrate the system at densities close to full packing. We show that, with increasing density, the system undergoes two entropy-driven phase transitions with two broken-symmetry phases. At low densities, the system is in a disordered phase. As intermediate phases, there is a solidlike sublattice phase in which one type of particle is preferred over the other and the particles preferentially occupy one of four sublattices, thus breaking both particle symmetry as well as translational invariance. At even higher densities, the phase is a columnar phase, where the particle symmetry is restored, and the particles preferentially occupy even or odd rows along one of the three directions. This phase has translational order in only one direction, and breaks rotational invariance. From finite-size scaling, we demonstrate that both the transitions are first order in nature. We also show that the simpler system with only one type of particle undergoes a single discontinuous phase transition from a disordered phase to a solidlike sublattice phase with an increasing density of particles.

I. INTRODUCTION

The study of the phases and critical behavior of lattice systems of hard particles having different geometrical shapes has been of continued interest in classical statistical mechanics, not only from the point of view of how complex phases arise from simple interactions, but also for understanding how different universality classes of continuous phase transitions depend on the shape of the particles. Such hard core lattice gas (HCLG) models have also been of interest in the context of the freezing transition [1,2], directed and undirected lattice animals [3–5], the Yang-Lee edge singularity [6], and in the absorption of molecules onto substrates [7–11]. Since only excluded volume interactions are present, temperature plays no role, and phase transitions, if any, are entropy driven. Many different shapes have been studied in the literature. Examples include triangles [12], squares [13–19], dimers [20–23], mixtures of squares and dimers [24,25], Y-shaped particles [26,27], tetrominoes [28,29], rods [30–33], rectangles [34–37], disks [38,39], and hexagons [40]. The hard hexagon model on the triangular lattice is the only solvable model.

In this paper, we focus on hard Y-shaped particles on the triangular lattice. Particles with this shape arise in different contexts. A well-known example is immunoglobulin-G (IgG), an antibody present in human blood, consisting of four peptide chains, two identical heavy chains and two identical light chains [41]. IgG has many therapeutic usages and the study of different phases of Y-shaped particles [26,27,42] is important to understand the effect of density on the viscosity of the liquid. Another example of a Y-shaped particle that is relevant for applications is trinaphthylene. It has been useful to create a NOR logic gate on an Au(111) surface [43,44], in which naphthylene branches of the molecule come in contact with the Au atom and act as the input of the logic gate.

Motivated by these applications, there have been a few numerical studies [26,27] of systems of Y-shaped particles on a triangular lattice. Each particle constitutes a central site and three of its nearest neighbors chosen alternately. There are two types of particles possible depending on which of the neighbors are chosen. In Refs. [26,27], in addition to the hard core constraint, there are additional attractive interactions between the arms of neighboring particles. At low temperatures, a single first-order phase transition from a disordered phase to a high-density ordered phase was observed. The high-density phase consists of mostly only one of the two types of Y-shaped particles, and has a solidlike sublattice order. For temperatures above a critical temperature, there are no density-driven phase transitions [26,27]. At the critical temperature, the transition has been argued to belong to the Ising universality class [27]. For Y-shaped particles with larger arm lengths, other phases are also seen [26].

In this paper, we determine the different phases and nature of the phase transitions when only excluded volume interactions are present, corresponding to the infinite temperature limit of the model studied in Refs. [26,27]. We show that

───────
*mdipanjan@imsc.res.in
†trisha.nath@theorie.physik.uni-goettingen.de
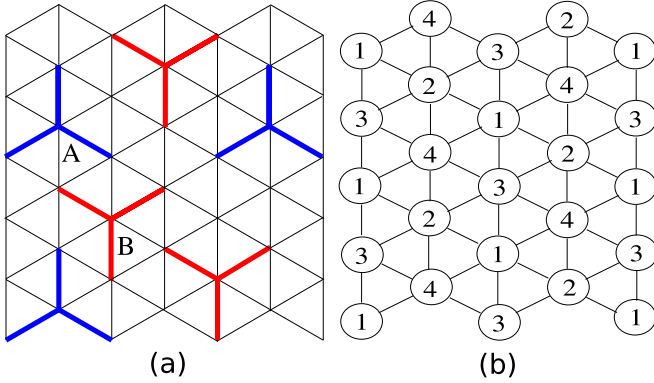‡rrajesh@imsc.res.in

FIG. 1. (a) Schematic diagram of a triangular lattice and the two types of Y-shaped particles. A- and B-type particles are represented by blue and red colors, respectively. (b) The lattice sites are labeled as 1,2,3,4 depending on the sublattice they belong to.

the sublattice phase at high densities which breaks particle symmetry is unstable to a sliding instability in the presence of vacancies. This results in the phase near full packing having columnar order, where there is translational order only in one of the three directions. This phase also has a roughly equal number of both types of particles. In the presence of attractive interactions between the arms of the particles, we argue, using a high-density expansion at finite temperatures, that this result continues to hold. Thus, irrespective of whether attractive interactions are present, neither does the high-density phase have sublattice order nor is there a critical temperature above which there is no phase transition, in contradiction to the results reported in Refs. [26,27]. We also demonstrate the presence of an intermediate phase, and that there are two entropy-driven phase transitions with an increasing density of particles: first, from a disordered phase to an intermediate-density sublattice phase where the symmetry between the two kinds of particles is broken, and second, from the sublattice phase to a high-density columnar phase where the symmetry between the two types of particles is restored. In addition, we also study the special case of the model when only one kind of Y-shaped particle is present, and show that it undergoes a single first-order transition from a disordered phase to an ordered sublattice phase.

The remainder of the paper is organized as follows. In Sec. II, we define the model precisely and explain the algorithm that we use to equilibrate the system in grand canonical Monte Carlo simulations. The different phases of the model and the nature of the phase transitions for systems with only one type of particle and both types of particles are numerically obtained in Secs. III and IV, respectively. Section V contains a summary and discussion of the results.

II. MODEL AND ALGORITHM

Consider a two-dimensional triangular lattice of linear dimension L with a periodic boundary, as shown in Fig. 1(a). A lattice site may be empty or occupied by one of two types of particles. Particles are Y shaped and occupy four lattice sites, consisting of a central site and three of its six neighbors chosen alternately. The three neighbors can be chosen in two different

ways, and hence there are two types of particles, examples of which are shown in Fig. 1(a). We will refer to the two types as A- and B-type particles. The particles interact through an excluded volume interaction, i.e., a site may be occupied by at most one particle. Activities $z_A = \exp(\mu_A)$ and $z_B = \exp(\mu_B)$ are associated with each A- and B-type particle, respectively, where μ_A and μ_B are the reduced chemical potentials. We will refer to the central site of a particle as its head.

We study the system using grand canonical Monte Carlo simulations. Conventional algorithms involving local evaporation and deposition of a single particle are inefficient in equilibrating the system at densities close to full packing. We implement an improved version of a recently introduced algorithm with cluster moves that is able to efficiently equilibrate systems of particles with large excluded volume interactions at densities close to full packing [31,45], as well as at the fully packed density [24].

We briefly describe the algorithm. First, a row is chosen at random (the row can be in any of the three directions of the triangular lattice). Then all the A-type (or equivalently B-type) particles with heads on this row are evaporated. The row now consists of empty intervals separated from each other by B-type particles with heads on the same row as well as A- and B-type particles with heads on neighboring rows. These empty intervals are now reoccupied with A-type particles with the correct equilibrium probabilities. The calculation of these probabilities reduces to determining the partition function of a one-dimensional system of dimers. Details may be found in Refs. [24,31,39,45]. For each row, we choose at random whether A- or B-type particles are to be evaporated. A Monte Carlo move is completed when $3L$ rows are updated.

Though the above algorithm is able to equilibrate the system at densities close to full packing, we find that the equilibration times as well as the autocorrelation times are large. In order to improve the efficiency of the algorithm, we introduce a sliding move in addition to the evaporation-deposition move. The first step in the sliding move is to select a site at random. If the site is not occupied by the head of a particle, then another site is chosen. If the site is occupied by the head of a particle, then one direction out of six possible directions is chosen, and we identify a cluster of the same type of particles, defined as a set of consecutive particles separated by two sites, starting from the randomly chosen site along the chosen direction. An example of such a cluster is shown by the highlighted box in Fig. 2(a). The cluster of particles is slid by one lattice site in the chosen direction and the particle type is changed from $A \leftrightarrow B$ [see Fig. 2(b)]. The new configuration is accepted if it does not violate the hard core constraint. It is straightforward to confirm that the sliding move obeys a detailed balance as the reverse move occurs with exactly the same probability. A Monte Carlo move is completed when $3L$ rows are updated through the evaporation-deposition move and $L^2/10$ sliding moves are attempted. We have chosen a ratio of sliding to evaporation-deposition moves that is efficient but has not optimized the ratio.

We compare the efficiency of the algorithm with and without the sliding move in Fig. 3. Starting from a disordered phase, the system is evolved in time at a value of chemical potential $\mu = \mu_A = \mu_B$ for which the equilibrium density is high (≈ 0.967), and the system is ordered. From Fig. 3, we
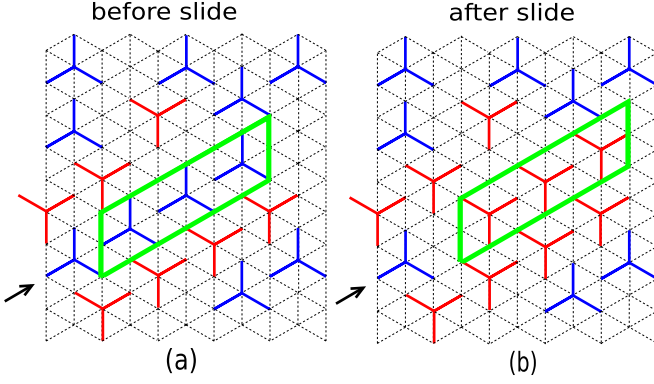
FIG. 2. Schematic diagram to illustrate the sliding move. A cluster is identified [highlighted box in (a)] by randomly choosing a site and one of the six directions (shown by arrow). The cluster is slid by one lattice site in the chosen direction and the particle type is switched from $A \leftrightarrow B$ to obtain a new configuration as shown in (b).

FIG. 4. Snapshot of typical equilibrated configurations of the system obtained from *grand canonical* Monte Carlo simulations with only one type of particle ($z_A = 0$) for two different values of chemical potential: (a) Disordered phase at $\mu_B = 1.420$ ($\rho^B \approx 0.710$) and (b) sublattice phase at $\mu_B = 1.765$ ($\rho^B \approx 0.775$). The particles on the four sublattices 1, 2, 3, and 4 are represented by green, red, blue, and magenta, respectively. The data are for a system of size $L = 300$.

see that the density reaches the equilibrium value in 10^5 steps when the sliding move is present compared to 4×10^6 steps when the sliding move is absent. Second, we calculate the density-density autocorrelation function, defined as

$$C(t) = \frac{\langle \rho(t + t_0)\rho(t_0)\rangle - \langle\rho\rangle^2}{\langle\rho^2\rangle - \langle\rho\rangle^2},\tag{1}$$

where $\rho(t)$ is the density at time t, and the average is over t_0. We determine the autocorrelation time τ by fitting the correlation function to an exponential,

$$C(t) \approx e^{-t/\tau}.\tag{2}$$

From the inset of Fig. 3, we find the autocorrelation time τ_{ws} for the algorithm with a sliding move is $\tau_{ws} \approx 82$, while the autocorrelation time τ_{ns} for the algorithm with no sliding move is $\tau_{ns} \approx 731$. Thus, the inclusion of the sliding move

results in considerably shorter equilibration times as well as autocorrelation times, and results in much better statistics. We have also checked that the autocorrelation function is independent of different choices of t_0, showing that time translational invariance has been achieved and the system has equilibrated.

The evaporation and deposition of particles along a row depends only on the configuration of the four neighboring rows. Thus, rows that are separated by three can be updated simultaneously, and the implementation of the algorithm is easily parallelizable. All the results presented in this paper are obtained using the parallelized algorithm. Equilibration is checked by starting the simulations with different initial conditions, corresponding to different phases, and confirming that the equilibrated phase is independent of the initial condition.

III. ONE TYPE OF PARTICLE ($z_A = 0$)

We first obtain the phase diagram for the case when only B-type particles are present, corresponding to $z_A = e^{\mu_A} = 0$ and $z_B = e^{\mu_B} > 0$. To demonstrate the different types of phases present in the system, we divide the lattice into four sublattices as shown in Fig. 1(b). A particle occupies four sites that belong to four different sublattices. We color the four sites occupied by a particle by one of four colors depending on the sublattice that the head of the particle belongs to. Snapshots of typical equilibrated configurations are shown in Fig. 4 for both small densities [Fig. 4(a)] and high densities [Fig. 4(b)]. From the snapshots, it is clear that at small densities, all four colors are roughly equally present. We will refer to this phase as the disordered phase, in which

$$\rho_1^B \approx \rho_2^B \approx \rho_3^B \approx \rho_4^B, \quad \text{disordered phase},\tag{3}$$

where ρ_i^B is the fraction of sites in sublattice i that are occupied by B-type particles.

The snapshot of the system at higher densities, as shown in Fig. 4(b), is predominantly of one color, implying that the heads of the particles preferably occupy one of the four sublattices.
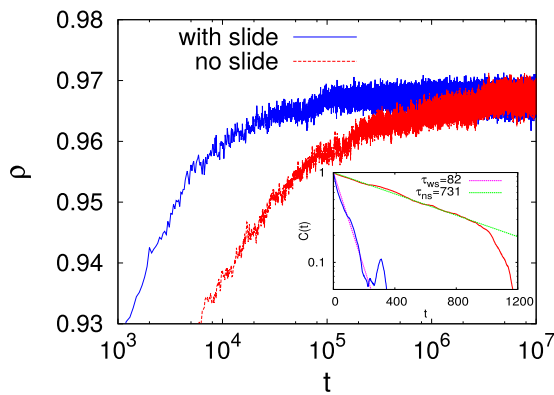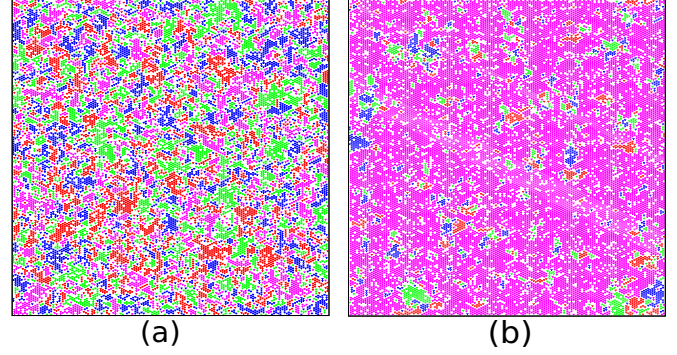

FIG. 3. The increase in density ρ to its equilibrium value for a system of size $L = 300$ and $\mu = \mu_A = \mu_B = 6.0$ for the algorithms with (blue) and without (red) the sliding move. The initial condition is disordered and the equilibrium configuration has $\rho \approx 0.967$, and is ordered. A logarithmic scale has been used for the t axis. Inset: Equilibrium density-density autocorrelation function $C(t)$ as a function of time t. When fitted to an exponential as in Eq. (2), we obtain $\tau_{ws} \approx 82$ when the sliding move is present and $\tau_{ns} \approx 731$ when the sliding move is absent.
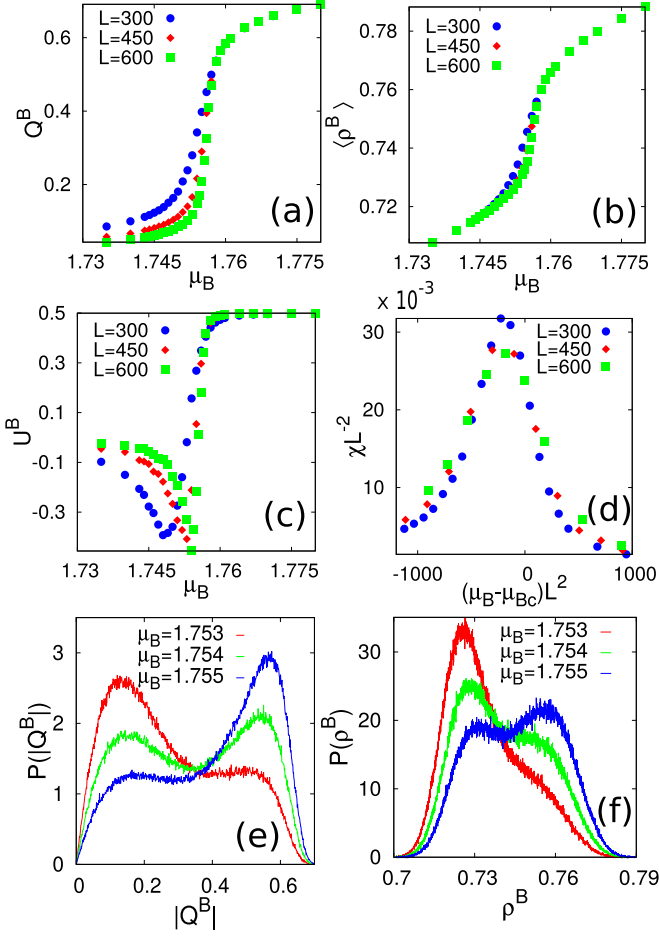
FIG. 5. Plot of (a) order parameter Q^B, (b) total density ρ^B, (c) Binder cumulant U^B, and (d) χL^{-2}, as a function of chemical potential μ_B for three different system sizes $L = 300$ (blue), 450 (red), and 600 (green). Plot of probability density function (e) $P(|\mathbf{Q^B}|)$, (f) $P(\rho^B)$ for $\mu_B = 1.753$, 1.754, and 1.755 with system size $L = 300$.

We will refer to this solidlike phase as the sublattice phase. The sublattice phase has translational order.

To quantify the phase transition from the disordered phase to sublattice phase, we define the vector

$$\mathbf{Q}^B = |Q^B|e^{i\theta_B} = \sum_{n=1}^{4} \rho_n^B e^{i(n-1)\pi/2}, \qquad (4)$$

where the sublattice densities ρ_i^B are as defined in Eq. (3). We define the sublattice order parameter Q^B to be

$$Q^B = \langle|\mathbf{Q}^B|\rangle, \qquad (5)$$

where the average $\langle\cdots\rangle$ is over equilibrium configurations. Clearly, Q^B is zero in the disordered phase and nonzero in the sublattice phase.

The variation of Q^B with chemical potential μ_B is shown in Fig. 5(a) for different system sizes. It increases sharply from zero to a nonzero value as μ_B crosses a critical value $\mu_{Bc} \approx 1.75$ and critical density $\rho_c^B \approx 0.750$. The transition becomes sharper with increasing system size. The total density of the system ρ^B has a system size dependence for intermediate densities [see Fig. 5(b)]. We also study the Binder cumulant
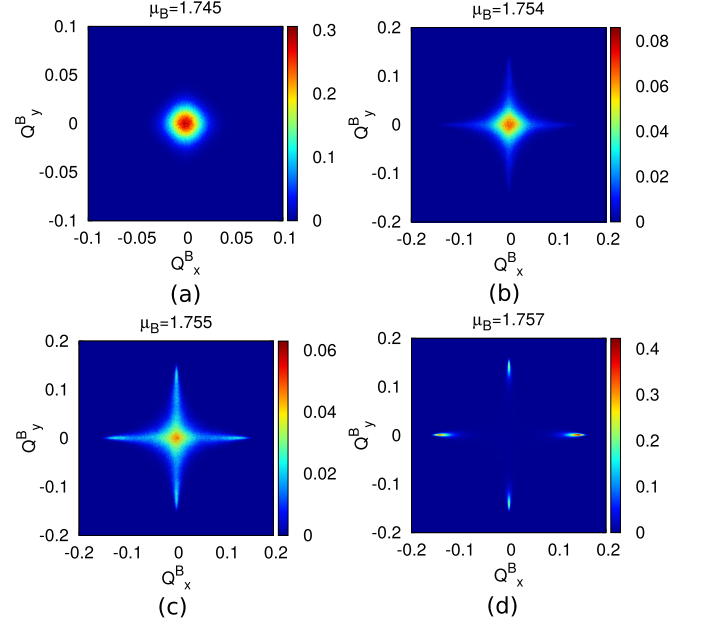

FIG. 6. Two-dimensional density plots of $P(\mathbf{Q^B})$ for different values of μ_B near the transition: (a) $\mu_B = 1.745$, (b) $\mu_B = 1.754$, (c) $\mu_B = 1.755$, and (d) $\mu_B = 1.757$. The data are for a system of size $L = 600$.

U^B defined as

$$U^B = 1 - \frac{\langle|\mathbf{Q}^B|^4\rangle}{2\langle|\mathbf{Q}^B|^2\rangle^2}. \qquad (6)$$

The variation of U^B with μ_B is shown in Fig. 5(c) for three different system sizes. For small μ_B, it is zero for the disordered phase and close to 0.5 for the ordered phase, as expected. Near the transition point, U^B becomes negative and the minimum value decreases with increasing system size. This is a clear signature of a first-order transition, as for a continuous transition U^B is positive and the data for different system sizes intersect at the critical point. We conclude that the transition is first order. Now, consider the susceptibility χ defined as

$$\chi = L^2(\langle|\mathbf{Q}^B|^2\rangle - Q^{B^2}). \qquad (7)$$

For a first-order transition, the singular behavior of χ near the transition obeys the finite-size scaling $\chi \sim L^2 f[(\mu_B - \mu_{Bc})L^2]$, where f is a scaling function. The data for χ for different system sizes collapse onto one curve when scaled as above with $\mu_{Bc} \simeq 1.756$, as shown in Fig. 5(d).

We now give further evidence of the transition being first order. At a first-order phase transition, the system keeps transiting from the disordered phase to the sublattice phase. This results in the probability distributions for the order parameter and density having multiple peaks. The probability distribution for $|\mathbf{Q^B}|$ and the density ρ^B are shown in Figs. 5(e) and 5(f), respectively, for values of μ_B near the transition point. The plots show two clear peaks for $\mu_B \approx 1.75$, one corresponding to the disordered phase and the other to the sublattice phase, consistent with a first-order transition. The two-dimensional color plot of the probability distribution of the complex order parameter $\mathbf{Q^B}$ near the critical point is shown in Fig. 6, and is consistent with the above observation.
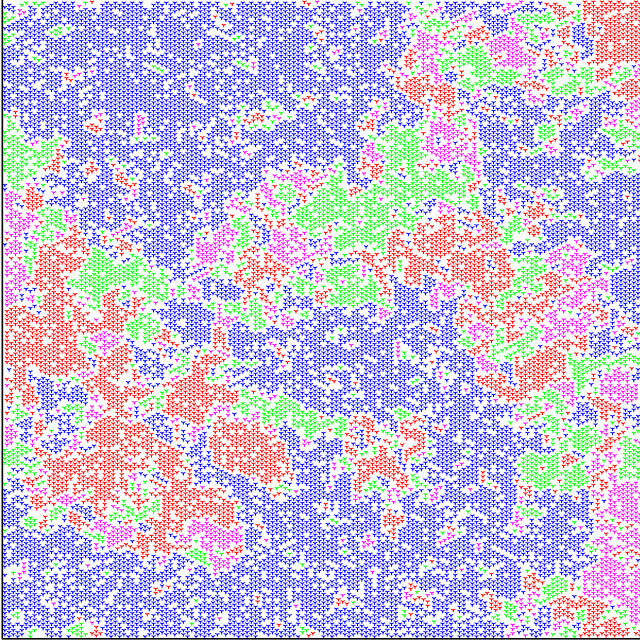
FIG. 7. Snapshot of a typical equilibrated configuration of the system obtained from *canonical* Monte Carlo simulations with one type of particle having fixed density $\rho^B = 0.740$. The particles on the four sublattices 1, 2, 3, and 4 are represented by green, red, blue, and magenta, respectively. The snapshot shows the coexistence of the sublattice and disordered phases. The data are for a system of size $L = 300$.

To further establish the first-order nature of the transition, we show coexistence of the disordered phase and sublattice phase at the transition point. To do so, we do simulations in the canonical ensemble, conserving density, of a system having density that lies between the density of the disordered system just below the transition and the density of the sublattice phase just above the transition. We choose $\rho^B = 0.74$, which lies between the two maxima of the probability distribution for density, as shown in Fig. 5(f). The system is evolved in time through an algorithm that conserves the density of the system. A lattice site is chosen at random. If it is occupied by the head of a particle, the particle is removed and deposited at another randomly chosen lattice site. If the deposition does not violate the hard core constraint, the move is accepted, else the particle is placed at its original position. The algorithm obeys a detailed balance as each move is reversible and occurs at the same rate. The snapshot of a typical equilibrated configuration of the system is shown in Fig. 7. There are regions where the color is uniform (blue), showing a sublattice phase, while there are other regions where all four colors appear, corresponding to a disordered phase. We conclude that there is phase segregation and coexistence, both signatures of a first-order transition.

IV. TWO TYPES OF PARTICLES ($z_A = z_B$)

Now consider the case where both types of particles are present with equal activity $z_A = z_B = z$. It is natural to expect that the fully packed phase has a sublattice order where the heads of particles occupy only one sublattice. We first argue that at densities close to full packing, sublattice order is not
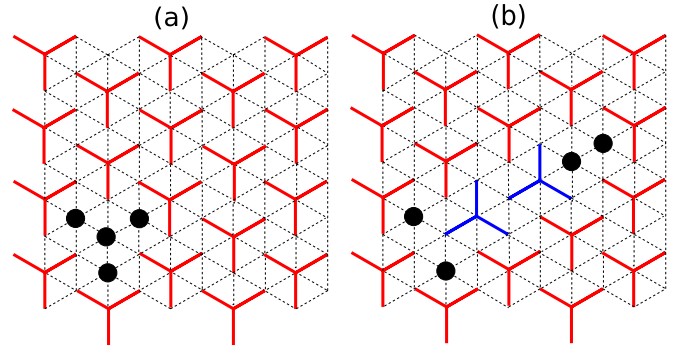

FIG. 8. (a) Schematic diagram showing the creation of a vacancy consisting of four empty sites (black solid circles), when a particle is removed from the fully packed sublattice phase. (b) The vacancy may be split into two half vacancies, and separated along a row by sliding particles along the row and changing the type.

stable due to the presence of vacancies, and the system prefers a columnar order with densities of both types of particles being roughly equal. We illustrate this instability through an example.

Consider a fully packed configuration with sublattice order. Such a configuration can have only one type of particle (say, B type). Removal of a single particle creates a single vacancy made of four empty sites, as shown by the solid circles in Fig. 8(a). These empty sites may be split into two unbound pairs of half vacancies by sliding a number of consecutive particles adjacent to the empty sites and flipping their type to A, each of these configurations having the same weight. An example of two particles being slid is shown in Fig. 8(b). Introducing more vacancies results in destabilizing the sublattice phase. Sliding results in restoring translational invariance along two of the three directions. However, translational order is still present in the third direction. We will refer to this phase as the columnar phase. We note that in this phase, two sublattices are preferentially occupied, one with A-type particles and the other with B-type particles. The stabilization of the columnar phase by creating vacancies is an example of order by disorder, a prototypical example being the hard square gas [13–17,19].

If additional attractive interactions are present between neighboring arms, then the above argument may also be extended to account for the energy cost of creating vacancies. It may then be shown that even for this case, that at high densities, the columnar phase is preferred over the sublattice phase, at all finite temperatures. To preserve continuity of presentation, we postpone the description of the generalized argument to Sec. V.

We now give numerical evidence for the high-density phase being columnar and also determine numerically the different phases of the system at densities away from full packing. Snapshots of equilibrated configurations of the system for different values of μ are shown in Fig. 9. Here, the lattice sites are colored using eight colors depending on the type of particle (two types) and sublattice (four sublattices) that the head belongs to. For small values of μ, the snapshot contains all eight colors distributed uniformly [see Fig. 9(a)], corresponding to the disordered phase. For intermediate values of μ, the snapshot shown in Fig. 9(b) is predominantly of one color. This phase corresponds to a sublattice phase. The
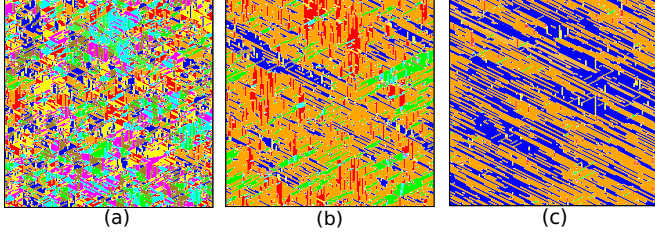
FIG. 9. Snapshots of equilibrated configurations of the system with two types of particles obtained from *grand canonical* Monte Carlo simulations for different values of μ: (a) Disordered phase with $\mu = 4.5$ ($\rho \approx 0.88$), (b) sublattice phase with $\mu = 5.4$ ($\rho \approx 0.947$), and (c) columnar phase with $\mu = 6.0$ ($\rho \approx 0.967$). The particles on the four sublattices 1, 2, 3, and 4 are represented by yellow, olive, cyan, and orange for type A and by green, red, blue, and magenta for type B. The data are for a system of size $L = 300$.

sublattice phase breaks the A-B symmetry and one type of particle is preferred over the other. Finally, for larger values of μ, the snapshot shown in Fig. 9(c) has mostly two colors that appear in strips. This phase corresponds to the columnar phase. This is in agreement with our argument presented above that the phase close to full packing is columnar due to the sublattice phase being unstable due to a sliding instability. We thus identify two phase transitions, the critical values of μ being denoted as μ^{DS} and μ^{SC}.

The sublattice phase has an eightfold degeneracy. To quantify it, consider the vector $\mathbf{Q}_s$,

$$\mathbf{Q}_s = |\mathbf{Q}^A| - |\mathbf{Q}^B|, \qquad (8)$$

where $\mathbf{Q}^B$ is given in Eq. (4) and $\mathbf{Q}^A$ has a similar definition with ρ_n^B replaced by ρ_n^A. We define the sublattice order parameter Q_s to be

$$Q_s = \langle |\mathbf{Q}_s| \rangle. \qquad (9)$$

Q_s is zero in the disordered phase and nonzero in the sublattice phase. It is also straightforward to check that $Q_s \approx 0$ in the columnar phase. We characterize the fluctuations of Q_s through the susceptibility χ_s defined as

$$\chi_s = L^2(\langle |\mathbf{Q}_s|^2 \rangle - Q_s^2). \qquad (10)$$

We also define the Binder cumulant associated with Q_s as U_s,

$$U_s = 1 - \frac{\langle |\mathbf{Q}_s|^4 \rangle}{2\langle |\mathbf{Q}_s|^2 \rangle^2}. \qquad (11)$$

To characterize the symmetry breaking between the two types of the particles in the disordered phase, we introduce an order parameter ρ_d defined as

$$\rho_d = \langle |\rho^A - \rho^B| \rangle, \qquad (12)$$

where ρ^A and ρ^B are the fraction of sites occupied by A- and B-type particles, respectively. We denote the associated susceptibility as χ_d and Binder cumulant as U_d,

$$\chi_d = L^2\left[\langle (\rho^A - \rho^B)^2 \rangle - \rho_d^2\right], \qquad (13)$$

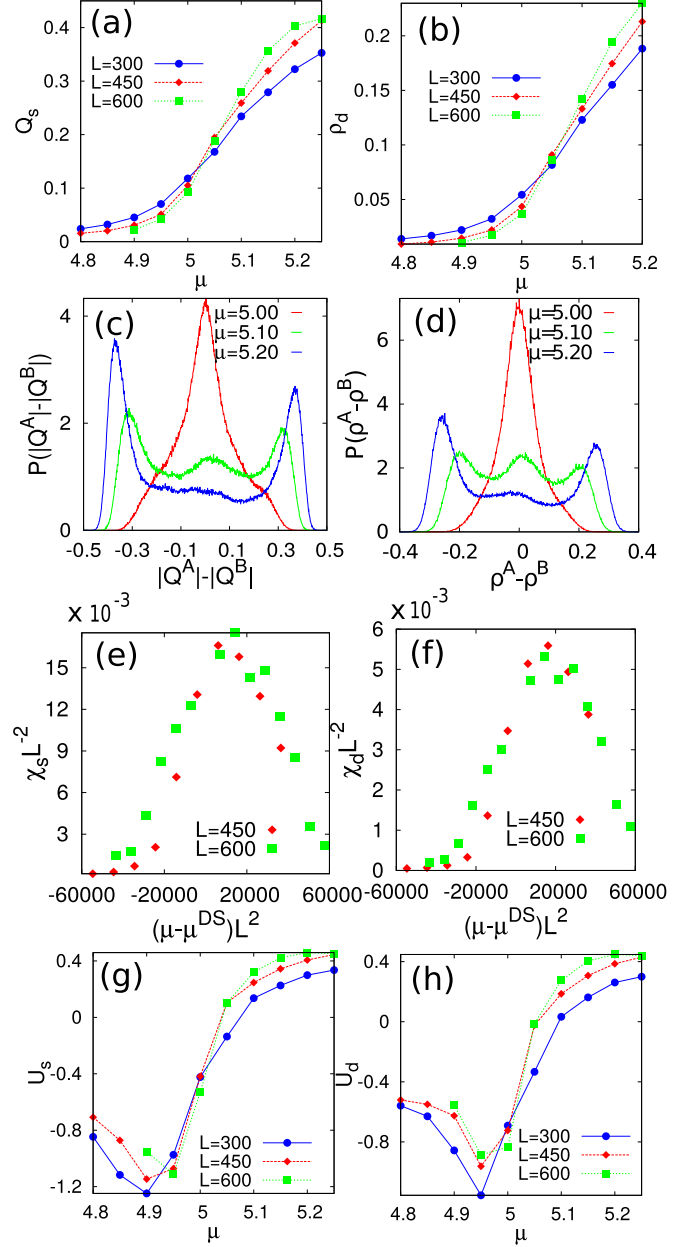$$U_d = 1 - \frac{\langle |\rho^A - \rho^B|^4 \rangle}{2\langle |\rho^A - \rho^B|^2 \rangle^2}. \qquad (14)$$

FIG. 10. Plot of (a) sublattice order parameter Q_s and (b) density difference ρ_d as a function of μ. Plot of probability distribution: (c) $P(|Q^A| - |Q^B|)$ and (d) $P(\rho^A - \rho^B)$ near disorder to the sublattice transition for a system of size $L = 300$. Plot of rescaled susceptibilities: (e) $\chi_s L^{-2}$ and (f) $\chi_d L^{-2}$ associated with Q_s and ρ_d, respectively about the critical point μ^{DS}. Plots are for systems of size $L = 300$, 450, and 600.

The variation of the order parameters Q_s and ρ_d with μ is shown in Figs. 10(a) and 10(b), respectively. They increase from close to zero to a nonzero value, showing the presence of the sublattice phase. The curves for different system sizes cross close to $\mu \approx 5.07$, and density $\rho \approx 0.930$. While a clear discontinuity in the order parameters is not discernible from Figs. 10(a) and 10(b), we now present evidence for the transition being first order in nature. The probability distributions for $\mathbf{Q}_s$ and $|\rho^A - \rho^B|$ near the transition point are shown in Figs. 10(c) and 10(d), respectively. As μ is

increased, the probability distributions change from being single peaked, corresponding to the disordered phase, to a three-peaked distribution, corresponding to a coexistence of the sublattice and disordered phase, to a symmetric double-peaked distribution, corresponding to the sublattice phase. Coexistence close to the transition is a clear signature of the first-order nature of the transition. We note that the distributions sharpen with increasing system size. The variation of Binder cumulant U_s and U_d with μ is shown in Figs. 10(g) and 10(h), respectively. It becomes negative for certain values of μ, which is a clear signature of a first-order transition. In a first-order transition, the susceptibilities scale as

$$\chi \sim L^2 f[(\mu - \mu_c)L^2]. \tag{15}$$

When scaled as described with $\mu^{DS} \approx 5.07$, $\rho^{DS} \approx 0.930$, the data for different system sizes collapse onto a single curve, as shown in Figs. 10(e) and 10(f). We conclude that the disordered to sublattice transition is first order in nature.

In the columnar phase, two sublattices are preferentially occupied by the particles. This selection can be done in six different ways and each way has two possibilities of filling, as A-type and B-type particles can choose either one of the selected two sublattices. Thus, the columnar phase has a 12-fold degeneracy. To quantify this phase illustrated in Fig. 9(c), we define a columnar order parameter Q_c as follows. In the columnar phase, the particles occupy alternate rows along one of the three orientations, and occupy all rows in the other two orientations. The breaking of the translational invariance in a direction is reflected in the difference in the density of heads between even and odd rows and is captured by

$$Q_1 = |\rho_1 + \rho_2 - \rho_3 - \rho_4|,$$
$$Q_2 = |\rho_1 + \rho_3 - \rho_2 - \rho_4|, \tag{16}$$
$$Q_3 = |\rho_1 + \rho_4 - \rho_3 - \rho_2|,$$

where ρ_i is the fraction of sites belonging to sublattice i that is occupied by a particle, irrespective of the type. In Q_1, $(\rho_1 + \rho_2)$ measures the density of occupied sites in odd horizontal rows [see Fig. 1(b)] and $(\rho_3 + \rho_4)$ the density of occupied sites in even horizontal rows. Thus, Q_1 is nonzero only when there is translational order along the horizontal rows, and similar interpretations hold for Q_2 and Q_3. Now, consider the vector

$$\mathbf{Q}_c = |\mathbf{Q}_c|e^{i\theta_c} = Q_1 + Q_2 e^{2\pi i/3} + Q_3 e^{4\pi i/3}. \tag{17}$$

We define the columnar order parameter to be

$$Q_c = \langle |\mathbf{Q}_c| \rangle. \tag{18}$$

In the columnar phase, Q_c is nonzero. In the disordered phase $Q_c \approx 0$, as each of the Q_i in Eq. (16) is approximately zero. In the sublattice phase, one sublattice is preferentially occupied and each of the Q_i in Eq. (16) becomes nonzero but approximately equal in magnitude, and hence again $Q_c \approx 0$. Thus, a nonzero Q_c is a signature for the columnar phase. We define the corresponding susceptibility as

$$\chi_c = L^2 \big(\langle |\mathbf{Q}_c|^2 \rangle - Q_c^2\big). \tag{19}$$

In the columnar phase the sublattice order parameter Q_s [see Eq. (9)] and the density difference ρ_d [see Eq. (12)] both becomes zero. The variation of Q_s and ρ_d with μ is shown in Figs. 11(a) and 11(b), respectively. The probability
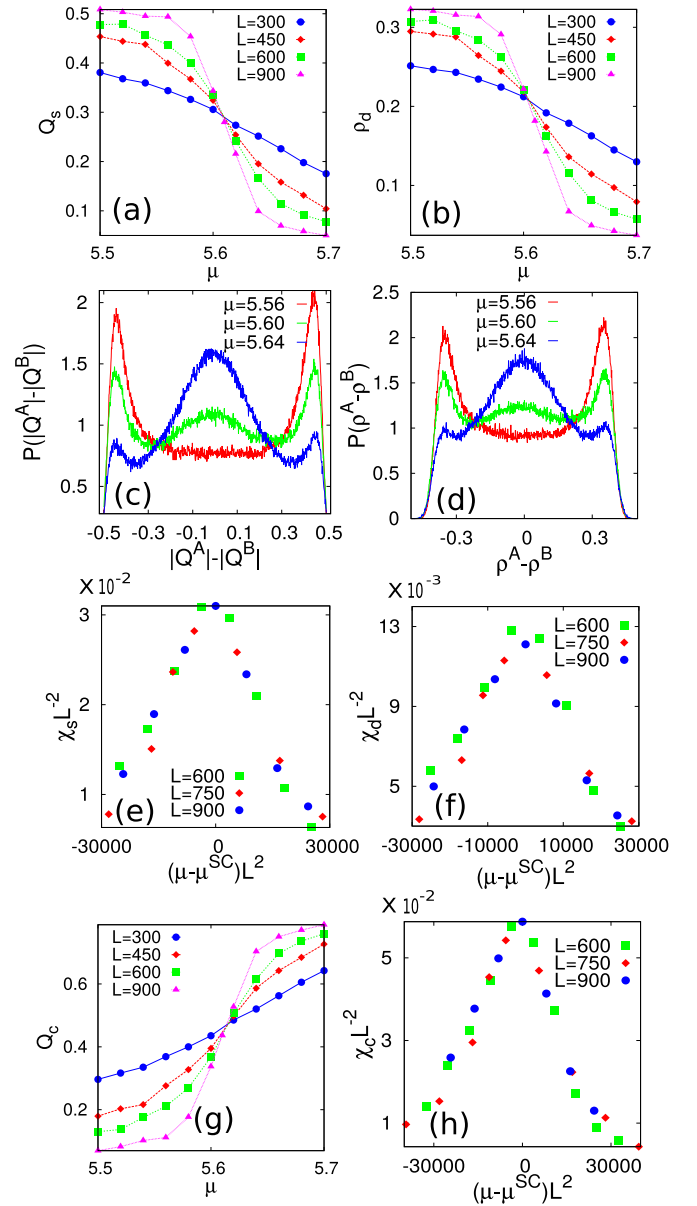

FIG. 11. Plot of (a) sublattice order parameter Q_s and (b) density difference ρ_d as a function of μ. Plot of probability distribution: (c) $P(|Q^A| - |Q^B|)$ and (d) $P(\rho^A - \rho^B)$ near the sublattice to columnar transition for the system size $L = 300$. Plot of rescaled susceptibilities: (e) $\chi_s L^{-2}$ and (f) $\chi_d L^{-2}$ associated with Q_s and ρ_d, respectively, about the critical point μ^{SC}. Plot of (g) columnar order parameter Q_c and (h) associated rescaled susceptibility $\chi_c L^{-2}$ as a function of μ and $(\mu - \mu^{SC})$, respectively. Plots are for systems of size varying from $L = 300$ to 900.

distributions for Q_s and $(\rho^A - \rho^B)$ near the transition point are shown in Figs. 11(c) and 11(d), respectively. As μ is increased, the probability distributions change from symmetric double-peaked, corresponding to the sublattice phase, to a three-peaked distribution, corresponding to a coexistence of the sublattice and columnar phase, to a dominant single-peaked distribution, corresponding to the columnar phase. The coexistence of both the columnar phase and sublattice phase is a signature of a first-order transition. For the first-order

transition susceptibilities follow the scaling law as described in Eq. (15). With this scaling we get the collapse of susceptibilities χ_s and χ_d onto a single curve, as shown in Figs. 11(e) and 11(f), for a critical value of the chemical potential $\mu^{SC} \approx 5.61$ with density $\rho^{SC} \approx 0.956$.

The variation of the order parameter Q_c with μ for different system sizes is shown in Fig. 11(g). It acquires a nonzero value in the columnar phase. The susceptibility χ_c also obeys the scaling law as described in Eq. (15). This is confirmed from Fig. 11(h) in which the collapse of curves for different system sizes with the described scaling is shown.

V. CONCLUSION

In this paper, we studied the different phases and phase transitions of hard Y-shaped particles on a two-dimensional triangular lattice. There are two types of Y-shaped particles depending on their orientation on the lattice, which are mirror images of each other. By incorporating cluster moves, we were able to equilibrate the system at densities close to full packing, allowing us to unambiguously determine the phases at all densities. In addition to the low-density disordered phase, we find two other phases. At intermediate phases, the phase has a solidlike sublattice order. In this phase, the symmetry between the two types of particles is broken, resulting in a majority of one type of particle. In addition, these particles preferentially occupy one of the four sublattices of the lattice. At high densities, the phase has columnar order. In this phase, the symmetry between the two types of particles is restored. However, there is translational order in one of the three directions, wherein particles preferentially occupy either even or odd rows. The first transition from the disordered to sublattice phase occurs at $\mu^{DS} \approx 5.07$ and the second transition from the sublattice to columnar phase occurs at $\mu^{SC} \approx 5.61$. Both the transitions are first order in nature. Y-shaped particles give a simple example of a system where a small number of vacancies destabilizes the sublattice phase into a columnar phase while a larger number of vacancies again stabilizes the sublattice phase. When only one type of particle is present, the model undergoes a single first-order phase transition from a low-density disordered phase to a high-density sublattice phase, and occurs at $\mu_{Bc} \approx 1.756$.

The high-density phase that we observe in this paper has columnar order with both types of particles equally present, which is in contradiction to the results obtained from Monte Carlo simulations of Y-shaped particles with attractive interactions in Refs. [26,27], wherein it was shown that the high-density phase has sublattice order in which only one kind of particle is present. For only excluded volume interactions, we argued in Sec. IV that the introduction of vacancies results in the destabilization of the sublattice phase into a columnar phase, because the vacancies split into two unbound half vacancies that can be separated away from each other, resulting in a gain in entropy. We now argue that this instability is present even in the presence of an attractive interaction between the nearest-neighbor arms of different particles. Consider the case when a vacancy is created by removing a single particle from a sublattice phase at full packing, as shown in Fig. 12(a). If $-\epsilon$ is the energy of each nearest-neighbor pair of arms, then this vacancy costs an energy 12ϵ. On splitting the vacancy into two
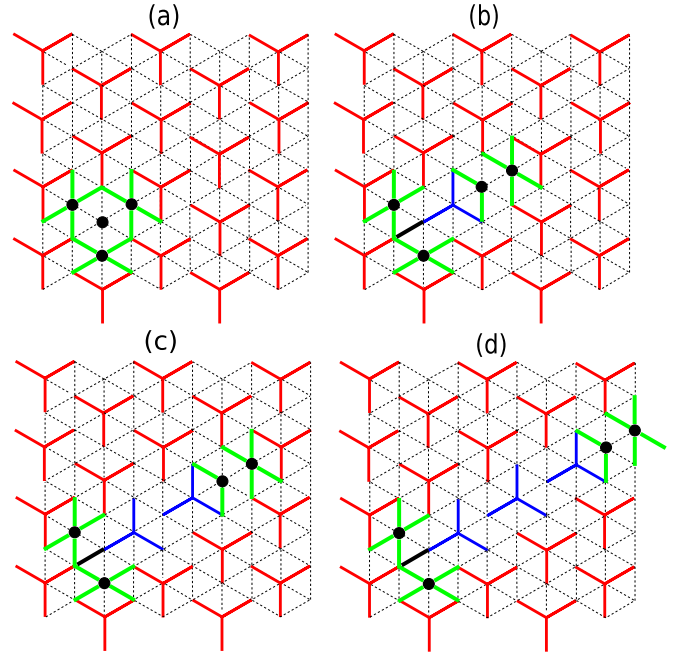

FIG. 12. Schematic diagrams to calculate, in a fully packed sublattice phase of B-type particles, the energy cost to create (a) a vacancy consisting of four empty sites (black solid circle), (b) two half-vacancies separated by one A-type particle, (c) two half vacancies separated by two A-type particles, and (d) two half vacancies separating three A-type particles. Compared to the background sublattice phase, green bonds increase the energy by ϵ while black bonds decrease the energy by ϵ. The energy cost is 12ϵ for (a), and 13ϵ for (b)–(d).

half vacancies and sliding them away from each other by one, two, or three particles [see Figs. 12(b)–12(d)], the energy cost increases to 13ϵ, but *does not* increase with separation between the half vacancies. Thus, the partition function Z of the system may be written as

$$Z = 4z^{N/4}e^{3N\beta\epsilon/2}\left[1 + \frac{Ne^{-12\beta\epsilon}}{4z} + \frac{3N\left(\frac{L}{2}-1\right)e^{-13\beta\epsilon}}{8z} + O(z^{-2})\right], \quad (20)$$

where $\beta = (kT)^{-1}$ is the inverse temperature. The free energy $\beta f = -\ln Z$ is then

$$\beta f = \frac{-\ln z}{4} - \frac{3\beta\epsilon}{2} - \frac{e^{-12\beta\epsilon}}{4z} - \frac{3Le^{-13\beta\epsilon}}{16z} + O(z^{-2}). \quad (21)$$

Clearly, the first-order correction term proportional to z^{-1} diverges with system size, as is indicative of systems with columnar order. If the divergent terms are resummed correctly, taking into account the columnar nature of the phase, then the first correction term becomes $O(z^{-1/2})$ [16,18]. The term of order z^{-1} being divergent implies that the expansion about the sublattice phase is not convergent, and thus we conclude that the high-density phase is columnar even when interactions are present. We note that in Ref. [26], attractive interactions were included for neighboring central sites, too. However, it may be

easily checked that the above expansion is true for this case also, albeit with an energy cost of 2ϵ for half vacancy when compared to bound vacancy. From Eq. (21), it may also be seen that for temperatures less than or of the order of $\epsilon/\ln L$, it would be possible to see a sublattice phase, but this is purely a finite-size effect.

In addition, it was argued in Refs. [26,27] that, for the model with attractive interactions and hard core constraints, there is no phase transition above a critical temperature. In the limit of infinite temperature, the attractive interactions play no role, and the model reduces to a problem with only hard core interactions between the particles, which is the model studied in the current paper. For the latter model, we established the presence of two density-driven phase transitions, in contradiction to the results implied in Refs. [26,27]. Reanalyzing the model with interactions to make the results consistent with those in the current paper is a promising area for future study. Another area for future study is the system of Y-shaped particles with larger arm lengths which could be symmetric [26]. For these systems with only an excluded volume interaction, we expect the high-density phase to be columnar [26].

It is tempting to analyze the high-density columnar phase using high-density expansions as developed for squares and rectangles [13–17,19,24,25]. These expansions are in terms of number defects (which could be extended). However, the columnar phase of Y-shaped particles is different from that of these simpler models, in which the types of particles occupy preferred sublattices in the columnar phase. This makes it difficult to even write the zeroth-order term for the partition function corresponding to no defects.

One may also consider kinds of lattices such as the honeycomb lattice. The honeycomb lattice (see Fig. 13) is different from the triangular lattice in that the site decides what type of Y molecule may be placed on it. We argue that the nature of the high-density phase is different on the honeycomb lattice as compared to the triangular lattice. Consider a fully packed phase, as shown in Fig. 13(a), in which translational order is broken, and the system is in a solidlike phase. Four vacancies may be created by removing one particle from site S_1, as shown in Fig. 13(b). The four vacant sites that are created remain bound to each other, and the solidlike order is stable. To next order in perturbation, consider creating eight vacant sites by removing two adjacent particles, as shown in Fig. 13(c). These eight vacancies may be split into two sets and moved arbitrarily far from each other by sliding particles along the direction shown by dotted lines in Fig. 13(c). This instability will lead to the phase becoming columnar (as argued by the high-density expansion for the triangular lattice). Thus, we have the following interesting scenario. As density is decreased from one, the system will first undergo a transition from a solidlike phase to a columnar phase. A further decrease in density may result in a transition to a solidlike phase as in
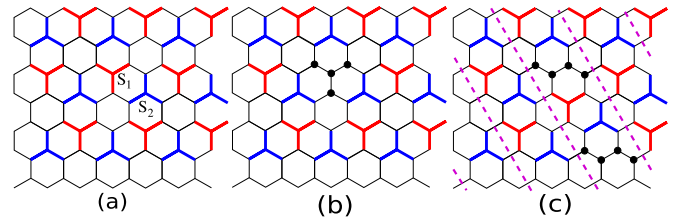

FIG. 13. Schematic diagrams of configurations on a honeycomb lattice when (a) no vacancy is present (full packing), (b) four bound vacancies are created by removing a particle from the site labeled S_1, and (c) eight unbounded vacancies are created by removing two particles from the sites labeled S_1 and S_2, followed by sliding particles in the directions shown by the dotted magenta lines. Black dots represent empty sites.

the triangular lattice followed by a disorder phase, or directly into a disordered phase. It would be interesting to verify these conjectures in Monte Carlo simulations.

HCLGs sometimes show multiple phase transitions with increasing density, but only when the excluded volume per particle is large. For instance, for multiple phase transitions to be present, the minimum range of interaction is seventh nearest neighbor for rods [31,33], fifth nearest neighbor for rectangles [34,35], fourth nearest neighbor for HCLG models for disks [18,39] while nearest-neighbor exclusion models such as the first-nearest-neighbor (1-NN) model on the square lattice [13,15,38,46–62] or the hard hexagon model on the triangular lattice [40] show only one transition from a disordered phase to a sublattice phase. The excluded volume of Y-shaped particles consists of nearest-neighbor sites, as in the hard hexagon model and half of the next-nearest-neighbor sites depending on the pair of particles being considered. It is quite surprising that despite the short-ranged nature of the interaction, the system undergoes two density-driven phase transitions. It is possible that this feature may also be extended to mixtures on a square lattice. From the insights gained from the current paper, we expect that if there are two kinds of particles A and B on a square lattice, where the A-A and B-B excluded volume interactions are up to second nearest neighbor, but the A-B excluded volume interaction is up to the third nearest neighbor, then the high-density phase will be columnar and there will be multiple transitions. Confirming this conjecture in simulations would be interesting.

[1] B. J. Alder and T. E. Wainwright, Phys. Rev. **127**, 359 (1962).

[2] B. J. Alder and T. E. Wainwright, J. Chem. Phys. **27**, 1208 (1957).

[3] D. Dhar, Phys. Rev. Lett. **49**, 959 (1982).

[4] D. Dhar, Phys. Rev. Lett. **51**, 853 (1983).

[5] D. C. Brydges and J. Z. Imbrie, J. Stat. Phys. **110**, 503 (2003).

[6] G. Parisi and N. Sourlas, Phys. Rev. Lett. **46**, 871 (1981).

[7] D. E. Taylor, E. D. Williams, R. L. Park, N. C. Bartelt, and T. L. Einstein, Phys. Rev. B **32**, 4653 (1985).

[8] A. Patrykiejew, S. Sokołowski, and K. Binder, Surf. Sci. Rep. **37**, 207 (2000).

[9] S. Mitchell, G. Brown, and P. Rikvold, Surf. Sci. **471**, 125 (2001).

[10] M. T. Koper, J. Electroanal. Chem. **450**, 189 (1998).

[11] P. Bak, P. Kleban, W. N. Unertl, J. Ochab, G. Akinci, N. C. Bartelt, and T. L. Einstein, Phys. Rev. Lett. **54**, 1539 (1985).

[12] A. Verberkmoes and B. Nienhuis, Phys. Rev. Lett. **83**, 3986 (1999).

[13] A. Bellemans and R. K. Nigam, J. Chem. Phys. **46**, 2922 (1967).

[14] A. Bellemans and R. K. Nigam, Phys. Rev. Lett. **16**, 1038 (1966).

[15] F. H. Ree and D. A. Chesnut, J. Chem. Phys. **45**, 3983 (1966).

[16] K. Ramola and D. Dhar, Phys. Rev. E **86**, 031135 (2012).

[17] T. Nath, D. Dhar, and R. Rajesh, Europhys. Lett. **114**, 10003 (2016).

[18] T. Nath and R. Rajesh, J. Stat. Mech. (2016) 073203.

[19] D. Mandal, T. Nath, and R. Rajesh, J. Stat. Mech. (2017) 043201.

[20] P. Kasteleyn, Physica **27**, 1209 (1961).

[21] H. N. V. Temperley and M. E. Fisher, Philos. Mag. **6**, 1061 (1961).

[22] D. A. Huse, W. Krauth, R. Moessner, and S. L. Sondhi, Phys. Rev. Lett. **91**, 167004 (2003).

[23] J. Nicholls, G. P. Alexander, and D. Quigley, arXiv:1702.01994.

[24] K. Ramola, K. Damle, and D. Dhar, Phys. Rev. Lett. **114**, 190601 (2015).

[25] D. Mandal and R. Rajesh, Phys. Rev. E **96**, 012140 (2017).

[26] P. Szabelski, W. Rzysko, T. Panczyk, E. Ghijsens, K. Tahara, Y. Tobe, and S. De Feyter, RSC Adv. **3**, 25159 (2013).

[27] D. Ruth, R. Toral, D. Holz, J. Rickman, and J. Gunton, Thin Solid Films **597**, 188 (2015).

[28] L. Mao, H. H. Harris, and K. J. Stine, J. Chem. Inf. Comput. Sci. **42**, 1179 (2002).

[29] B. C. Barnes, D. W. Siderius, and L. D. Gelb, Langmuir **25**, 6702 (2009).

[30] A. Ghosh and D. Dhar, Europhys. Lett. **78**, 20003 (2007).

[31] J. Kundu, R. Rajesh, D. Dhar, and J. F. Stilck, Phys. Rev. E **87**, 032103 (2013).

[32] A. Gschwind, M. Klopotek, Y. Ai, and M. Oettel, Phys. Rev. E **96**, 012104 (2017).

[33] N. Vigneshwar, D. Dhar, and R. Rajesh, J. Stat. Mech. (2017) 113304.

[34] J. Kundu and R. Rajesh, Phys. Rev. E **89**, 052124 (2014).

[35] J. Kundu and R. Rajesh, Phys. Rev. E **91**, 012105 (2015).

[36] T. Nath, J. Kundu, and R. Rajesh, J. Stat. Phys. **160**, 1173 (2015).

[37] P. Gurin, S. Varga, M. González-Pinto, Y. Martínez-Ratón, and E. Velasco, J. Chem. Phys. **146**, 134503 (2017).

[38] H. C. M. Fernandes, J. J. Arenzon, and Y. Levin, J. Chem. Phys. **126**, 114508 (2007).

[39] T. Nath and R. Rajesh, Phys. Rev. E **90**, 012120 (2014).

[40] R. J. Baxter, J. Phys. A **13**, L61 (1980).

[41] C. Janeway, *Immunobiology Five*, Vol. 1 of *Immunobiology 5: The Immune System in Health and Disease* (Garland Publishing, New York, 2001).

[42] J. Li, R. Rajagopalan, and J. Jiang, J. Chem. Phys. **128**, 205105 (2008).

[43] W. H. Soe, C. Manzano, N. Renaud, P. de Mendoza, A. De Sarkar, F. Ample, M. Hliwa, A. M. Echavarren, N. Chandrasekhar, and C. Joachim, ACS Nano **5**, 1436 (2011).

[44] S. Godlewski, M. Kolmer, H. Kawai, B. Such, R. Zuzak, M. Saeys, P. de Mendoza, A. M. Echavarren, C. Joachim, and M. Szymonski, ACS Nano **7**, 10105 (2013).

[45] J. Kundu, R. Rajesh, D. Dhar, and J. F. Stilck, AIP Conf. Proc. **1447**, 113 (2012).

[46] P. A. Pearce and K. A. Seaton, J. Stat. Phys. **53**, 1061 (1988).

[47] K. Binder and D. P. Landau, Phys. Rev. B **21**, 1941 (1980).

[48] D. S. Gaunt and M. E. Fisher, J. Chem. Phys. **43**, 2840 (1965).

[49] R. J. Baxter, I. G. Enting, and S. K. Tsang, J. Stat. Phys. **22**, 465 (1980).

[50] A. Baram and M. Fixman, J. Chem. Phys. **101**, 3172 (1994).

[51] L. K. Runnels, Phys. Rev. Lett. **15**, 581 (1965).

[52] L. K. Runnels and L. L. Combs, J. Chem. Phys. **45**, 2482 (1966).

[53] R. Nisbet and I. Farquhar, Physica **73**, 351 (1974).

[54] W. Guo and H. W. J. Blöte, Phys. Rev. E **66**, 046140 (2002).

[55] Y. B. Chan, J. Phys. A **45**, 085001 (2012).

[56] I. Jensen, J. Phys. A **45**, 508001 (2012).

[57] H. Meirovitch, J. Stat. Phys. **30**, 681 (1983).

[58] C. K. Hu and K. S. Mak, Phys. Rev. B **39**, 2948 (1989).

[59] D. J. Liu and J. W. Evans, Phys. Rev. B **62**, 2134 (2000).

[60] L. Lafuente and J. A. Cuesta, Phys. Rev. E **68**, 066120 (2003).

[61] Z. Ràcz, Phys. Rev. B **21**, 4012 (1980).

[62] C. K. Hu and C. N. Chen, Phys. Rev. B **43**, 6184 (1991).